Sensors and Actuators B 236 (2016) 490–498

Contents lists available at ScienceDirect

Sensors and Actuators B: Chemical

journal homepage: www.elsevier.com/locate/snb

Fabrication of lotus-like Au@TiO_2 nanocomposites with enhanced gas-sensing properties

Haiyang Liu, Wei Yang, Mingxi Wang, Li Xiao, Shantang Liu*

Key Laboratory for Green Chemical Process of Ministry of Education, Hubei Key Lab of Novel Reactor & Green Chemical Technology, School of Chemistry and Environmental Engineering, Wuhan Institute of Technology, Wuhan, 430073, PR China

ARTICLE INFO

Article history:
Received 17 December 2015
Received in revised form 25 May 2016
Accepted 6 June 2016
Available online 7 June 2016

Keywords:
Lotus-like Au@TiO_2
Hydrothermal method
Gas-sensing
Catalytic effect

ABSTRACT

The structure of lotus-like Au@TiO_2 was directly fabricated via a simple and cost-effective hydrothermal method by carefully adjusting the molar ratio of Au to TiF_4 in the precursor. (*) The crstal structure and morphology of the obtained louts-like Au@TiO_2 were examined by X-ray diffraction (XRD), transmission electron microscope (TEM), high resolution transmission electron microscope (HRTEM), Brunauer-Emmett-Teller (BET) and X-ray photoelectron spectroscopy (XPS). The results indicated that perfect lotus-like Au@TiO_2 hierarchical structure with Au pistil and TiO_2 petal can be formed when the molar ratio of Au to TiF_4 was 0.1875. Furthermore, the gas sensing test of the Au@TiO_2 nanocomposites towards CO gas was also examined. The responses of the Au@TiO_2-based sensors were higher than the pure TiO_2-based sensor. Especially, the lotus-like 18.75 mol%Au@TiO_2-based sensor presented a most outstanding gas sensing performance, including low optimal operating temperature, high sensitivity and selectivity as well as fast response and recovery time. Such sensing performance enhancement are ascribed to their unique lotus-like structures and the catalytic effect of the encapsulated Au nanoparticles (NPs).

1. Introduction

To meet the growing awareness about environmental pollution and safety issues, considerable efforts are being made to develop high-performance gas sensors for detecting toxic gases, supervising air quality and protecting human health [1,2]. As the key component of gas sensor, sensing materials determine the performance of a gas sensors, and draw many focus in the sensors research [3]. Semiconducting metal oxides have attracted intensive attention due to their cost efficiency, high sensitivity, and wide range response to various gases [2,4]. Several semiconducting oxides such as SnO_2 [5], ZnO [6], Fe_2O_3 [7], In_2O_3 [8], WO_3 [9] have been employed as gas sensors for detecting different kinds of gases. It has been confirmed that sensing property of semiconductor-oxides gas sensors is affected by their morphologies, microstructures and compositions [10–12]. Therefore, constructing novel types of semiconductor metal oxides with subtle hierarchically complex structures or configuration is primary importance for achieving desirable sensing performance.

As one kind of crucial semiconducting metal oxides, TiO_2 has found many applications ranging from photocatalysis [13], solar energy conversion [14], photo-induced hydrophilicity [15] to photochromic devices [16] and etc., because TiO_2 nanomaterials possess unique characterisitics in optical, electronic, chemical and physical fields. Furthermore, they are nontoxic, environmentally friendly, cost-effective, excellently biocompatible and stable, which let TiO_2 be a promising materials for use in gas sensors [17]. As a gas-sening material, TiO_2 has been applied in the detection of CO [18], H_2S [19], alcohol [20], H_2 [21], NO_x [22], etc. However, there still remains several drawbacks including long recovery time, high operating temperature (~300 °C) or low sensitivity at low temperature [23,24], which limit further applications of TiO_2 in sensors. In order to overcome these inherent limitations or improve its gas sensing performance, TiO_2 is usually deposited some noble metals or decorated by introducing exotic nanostructures. Up to now, diverse types of nanostructured TiO_2, for instance, thin films [25], nanobelts [26] and nanotubes [27] and three dimensional nanostructures TiO_2 [20] have been synthesized and used in gas sensors, and their sensing properties were accordingly enhanced dramatically. Nevertheless, only a few noble metal cores@TiO_2 nanocomposites have been prepared applying in gas sensors.

Herein, we present a strategy for enhancing the gas-sensing performance of TiO_2 nanomaterials by encapsulating Au NPs. The

* Corresponding author.
E-mail address: stliu@wit.edu.cn (S. Liu).

http://dx.doi.org/10.1016/j.snb.2016.06.039
0925-4005/

novel lotus-like Au@TiO_2 nanostructrue was achieved by a facile, environmentally friendly and one-step hydrothermal approach. Moreover, the morphology evolution process of the lotus-like Au@TiO_2 was also probed in our case. Furthermore, to prove the potential application, the CO sensing behavior of the lotus-like Au@TiO_2 was carried out. The results implied that the sensor based on the lotus-like Au@TiO_2 showed a dramatically enhanced gas-sensing performances toward CO with lower operating temperature and high response. This is mainly attributed to the unique lotus-like structures and the catalytic effect of the encapsulated Au NPs.

2. Experimental

2.1. Synthesis of Au@TiO_2 nanocomposites

All of the chemical reagents utilized in this experiment were of analytical grade and used without further purification. A typical procedure for synthesizing flower-like Au@TiO_2 nanocomposites is carried out as in the literature [28,29] with minor modification. A certain amount of 0.01 M $HAuCl_4$ solution was dispersed in 4.5 mL 0.01 M sodium citrate solution. The mixture was stirred vigorously for 2 min and then 5.0 mL of 0.01 M ascorbic acid was added dropwise to reduce $HAuCl_4$ to metallic Au NPs. The mixture appeared turned orchid and then rapidly to reddish brown. 6.0 mL of 0.04 M TiF_4 solution was added after further stirring for about 5 min. The mixture was subsequently diluted to 90 mL with deionized water and transferred to Teflon-lined stainless steel autoclaves. The hydrothermal reaction was conducted at 180 °C for 48 h. After that, the precipitate was collected by centrifugation and washed with water and absolute ethanol in sequence, and finally dried at 80 °C. Au@TiO_2 nanocomposites with different molar ratio of Au to TiF_4 (1.25, 18.75 and 37.5 mol%) were successfully fabricated by controlling the volume of $HAuCl_4$, they were denoted as 1.25, 18.75 and 37.5 mol% Au@TiO_2, respectively. Pure TiO_2 NPs was also synthesized without adding $HAuCl_4$ solution according to the above methods for comparison.

2.2. Characterization

The crystalline phases of the as-synthesized products were characterized by X-ray powder diffraction (XRD) using a Shimadzu XRD-6000 X-ray diffraction meter with CuKα1 irradiation (λ = 0.15406 nm) at 40 kV and 20 mA over 2θ range from 20 to 80°. The morphologies and structures of the samples were recorded by transmission electron microscopy (TEM), and high resolution transmission electron microscopy (HRTEM, JEOL, JEM-2010). The distribution of elements in crystal was conducted on an energy dispersive X-ray spectrometer (EDX, JEOL, JSM-5510LV). N_2 adsorption-desorption isotherms were measured on a Micromeritics ASAP2020 system. Surface area was evaluated using a Brunauer-Emmett-Teller (BET) method. X-ray photoelectron spectroscopy (XPS, K-Alpha) was used to investigate the electronic structure of the surface of 18.75 mol%Au@TiO_2.

2.3. Sensor fabrication and gas sensing measurement

The as-prepared samples were further ground into fine powders and mixed with absolute ethanol in a weight ratio of 4:1 to form paste, then the paste was dropped onto the cleaned Al_2O_3 (10 mm × 20 mm × 0.635 mm) substrate with interdigitated gold electrodes to form a sensing film and its thickness is about 100 μm. The fabricated sensors are presented in Fig. 1(b). The prepared gas sensing element was then dried in air to remove the unwanted impurities, followed by annealing at 500 °C for 3 h. Finally, the sensor was obtained after aging at 300 °C for 48 h.

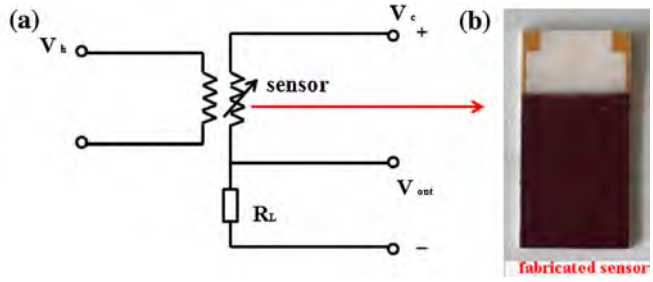

Fig. 1. (a) The circuit diagram for measuring the sensor resistance (b) A view of the fabricated sensor.

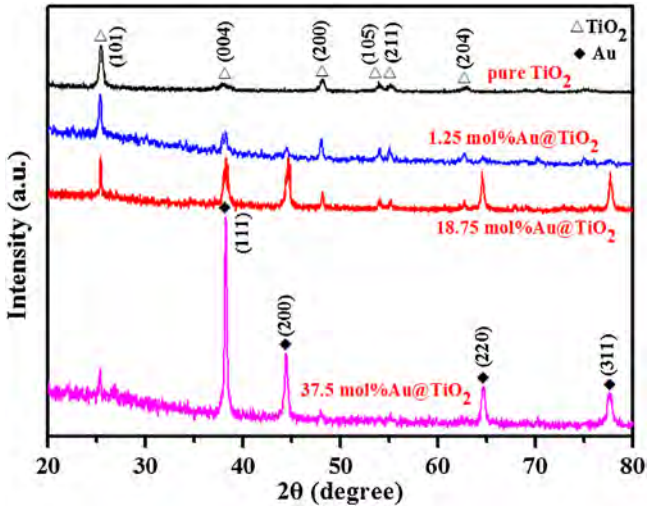

Fig. 2. X-ray diffraction patterns of as-prepared TiO_2 and Au@TiO_2 nanocomposites.

Gas sensing experiments were conducted on the CGS-1TP intelligent test system (Beijing Elite Tech. Co., Ltd., China). The sensor resistances are measured using the following circuit (Fig. 1(a)). The sensor is series with a load resistor (R_L) in a direct current (DC), and the circuit voltage (V_c) is constant in the measurement process. By monitoring the output voltage (V_{out}) of R_L, the resistance change of the sensor in air or the target gases can be obtained. The sensor resistance can be expressed using the formula: $R_{sensor} = (V_c - V_{out})R_L/V_{out}$.

The tested sensors were pre-heated at desired operating temperatures (200 ~ 400 °C) for about 30 min before injection the target gas. In process testing, corresponding gas were injected into the test box. As the resistance of the sensor was stable in air (R_a), the target gas was injected into the test chamber (18 L) by a micro injector, the resistance in the target gas (R_g) was achieved and recorded after the resistance reached new constant values. Here, the response of the as-prepared sensor is defined as R_a/R_g, and the response and recovery time were defined as the time taken by the sensor to achieve 90% of the total resistance change in the case of adsorption and desorption.

3. Results and discussions

3.1. Structural and morphological characteristics

The phase and structural analysis of the as-prepared final products are characterized by X-ray diffraction (XRD) and shown in Fig. 2. In the XRD patterns of pure TiO_2 sample, all of the peaks can be readily indexed to anatase phase TiO_2 (JCPDS No. 21-1272). A strong peak at 2θ of 25.30° corresponding to the (1 0 1) plane is clearly observed. With the introduction of $HAuCl_4$, the products

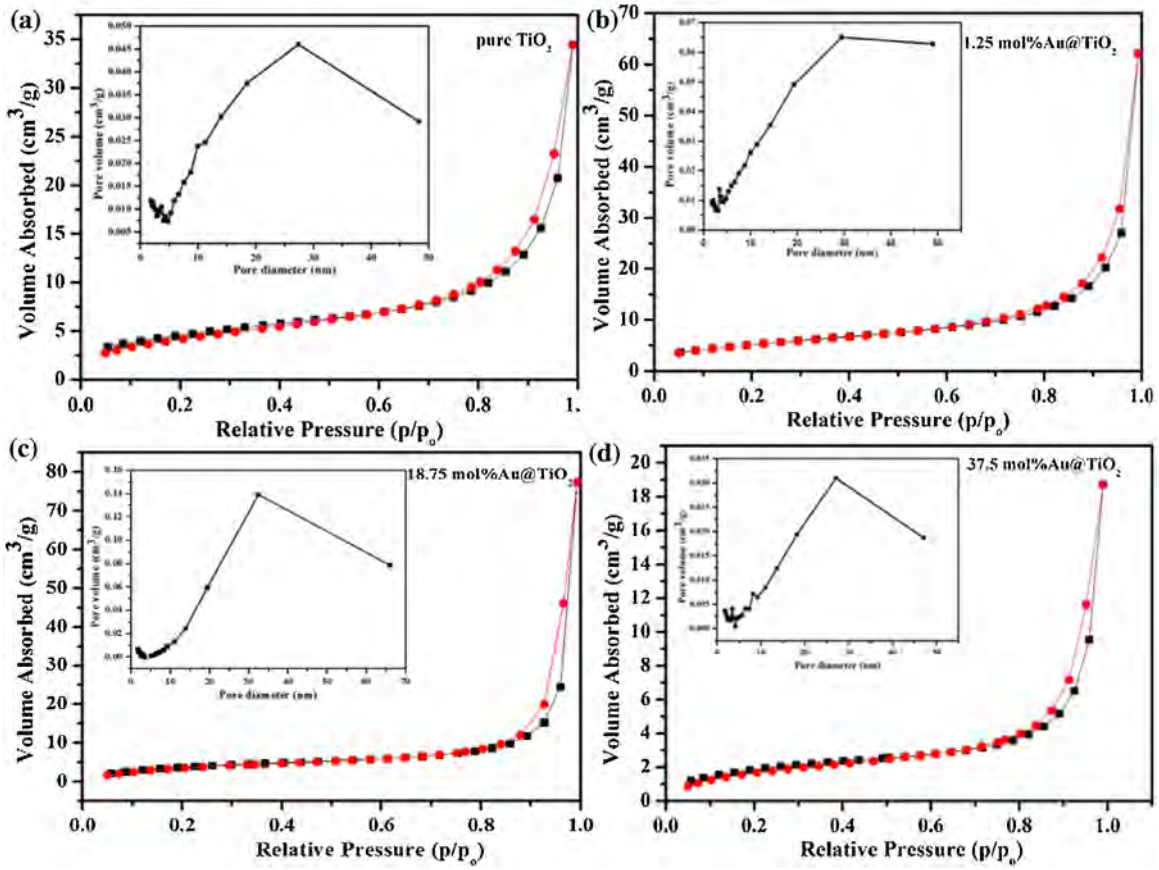

Fig. 3. Nitrogen adsorption-desorption isotherms of as-prepared TiO_2 and Au@TiO_2 nanocomposites.

Table 1
Surface area, pore volume, and pore diameter of the as-synthesized nanocomposites.

Sample	S_{BET}(m^2/g)	V_p(cm^3/g)	D_p (nm)
Pure TiO_2	16.35	0.05	13.52
1.25 mol%Au@TiO_2	19.04	0.09	19.16
18.75 mol%Au@TiO_2	14.91	0.12	30.80
37.5 mol%Au@TiO_2	6.99	0.03	18.69

show new XRD diffraction peaks marked with black diamond that are well assigned to Au (JCPDS No. 01-1174), which revealed the formation of Au@TiO_2 composites, no other peaks of impurity phase appeared. With the increase in Au content, the relative intensity of Au peaks enhanced dramatically, meanwhile the relative intensity of TiO_2 peaks marked with hollow triangles decreased.

Fig. 3. shows Nitrogen adsorption-desorption isotherms and Barrett-Joyner-Halenda (BJH) pore-size distribution plots of the as-synthesized nanocomposites at different Au contents. The samples show similar type-IV isotherms, which are representative of mesoporous solids. Detailed pore structure information is listed in Table 1. Nevertheless, all the samples display similar nitrogen dsorption-desorption isotherms and surface areas with wide pore-size distributions. The 18.75 mol%Au@TiO_2 has the largest pore volume and pore diameter.

The surface morphologies of pure TiO_2 and Au@TiO_2 nanocomposites synthesized with different ratio of Au/TiO_2 by hydrothermal method were investigated using TEM shown in Fig. 4. It is clearly seen that the morphology of these nanostructures is highly dependent on the contents of Au. Only leaf-like structures were observed in Fig. 4(a) for pure TiO_2 without Au, flower-like morphology began to develop and can be found in local domain in the sample of 1.25 mol%Au@TiO_2 (Fig. 4(b)). As the molar ratio of Au/TiO_2 rose to 0.1875, lotus-like structure was formed with uniform size and good monodispersity as illustrated in Fig. 4(c). When the content of Au continues to increase (37.5 mol%Au@TiO_2), the size of Au NPs will grow bigger resulting in destruction of the lotus-like structure displayed in Fig. 4(d). Energy dispersive X-ray analysis (EDX) was used to investigate the composition of pure TiO_2 (Fig. 4(e)) and 37.5 mol%Au@TiO_2 (Fig. 4(f)). The detected peaks in the EDX spectrum are assigned to Ti, O and Au respectively, no other impurities are detected in all samples. Based on Fig. 4(f). the components for Au and Ti are 12.81% and 21.98%, namely the molar ratio of Al/Ti in the sample is about 58%, exceeding to theoretical 37.5%. This may be attributed to the Energy dispersive X-ray analysis (EDX) is a semi-quantitative element analysis for the surface of the whole materials. Considering the results of XRD, EDX and TEM image, we can conclude that Au as a pistil is encapsulated in the center of lotus-like structure and TiO_2 acts as a petal. It is clearly demonstrated that 18.75 mol%Au@TiO_2 have an ideal lotus-like structure with pistil about 50 nm and petal of about 250 nm.

In order to gain further insight into the detailed growth information on the formation of the lotus-like Au@TiO_2 nanocomposites, HRTEM was employed to investigate the microstructures of lotus-like 18.75 mol%Au@TiO_2 and the results are depicted in Fig. 5. Fig. 5(b) shows the local crystalline lattices at the heterointerface of Au pistil and TiO_2 petal as marked by the rectangle in Fig. 5(a). The spacing between adjacent lattice fringes is 0.354 nm for TiO_2 petal, attributed to *d* spacing of the (1 0 1) crystal planes of anatase-type TiO_2 (*d* = 0.352 nm; JCPDS No. 21–1272). The interfringe distance is measured to be 0. 251 nm for the Au pistil displayed in Fig. 5(d), which is close to the d spacing of (1 1 1) planes of fcc metallic Au (d = 0.235 nm; JCPDS No. 01-1174). This reveals that (1 0 1) crystal planes of TiO_2 formed epitaxially near the Au@TiO_2 interface

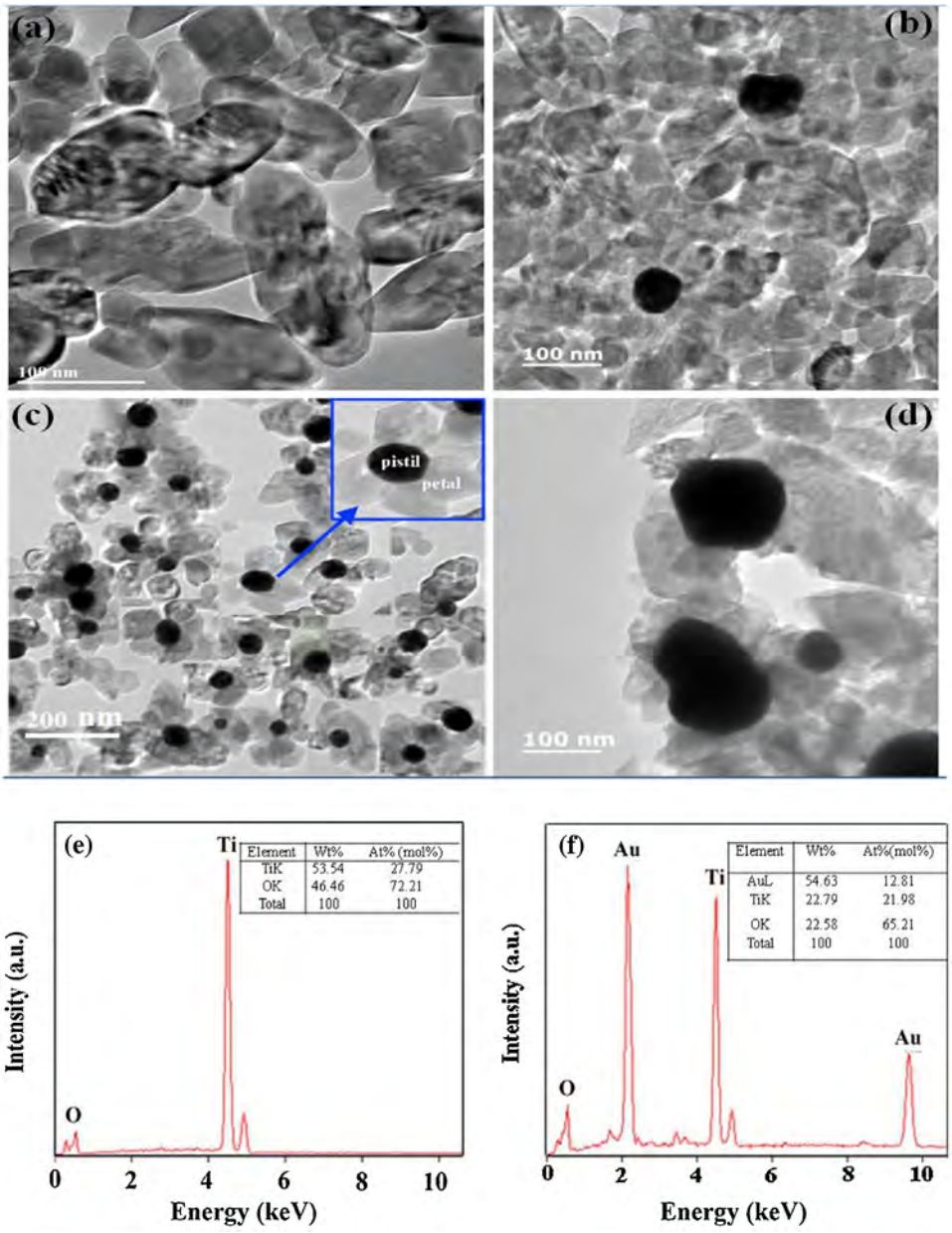

Fig. 4. TEM images for the as-prepared nanocomposites (a) pure TiO_2, (b) 1.25 mol%, (c) 18.75 mol%, (d) 37.5 mol%Au@TiO_2. (e) and (f) are the EDX spectra corresponding to (a) and (d), respectively.

due to matching with exposed Au (1 1 1) planes keeping interfacial energy low [30–32]. Compared with the root region, the interfringe distances of external edge is 0.241 nm shown in Fig. 5(c) indicated by the white circle in Fig. 5(a), attributed to the (0 0 4) plan (JCPDS No. 21-1272) of anatase type TiO_2, indicating that the petal TiO_2 crystals grow elongated along the [0 0 1] direction [29].

A previous study demonstrated that the crystallinity of Au seeds controlled the nucleation process [33,34]. Similarly, it is reasonable that the morphology of Au@TiO_2 was controlled by the contents of Au in this study. Exceed TiO_2 nanosheets gathered around smaller Au particles at low concentrations of $HAuCl_4$. With the increase of $HAuCl_4$ from 0.3 to 4.5 mL, Au NPs with acceptable size without particle aggregation and spherical shapes were formed, it is suitable for Au NPs provide perfect growth sits and multiple monocrystalline domains for TiO_2 to nucleation, resulting in the production of lotus-like heterostructures. As more $HAuCl_4$ was added, Au NPs aggregated seriously with changed surface state, which may hinder TiO_2 orientational growth. Only when the amount of $HAuCl_4$ was appropriate, the obtained Au particles possess uniformly spherical shape with proper size thus guiding uniform TiO_2 nanosheets growth, which contributes to this lotus-like heterostructures. As shown in Fig. 4, as the molar ratio of Au to TiF_4 changed from 0.0125, 0.1875–0.375, the size of Au in Au@TiO_2 composites was about 70, 50, 140 nm, respectively. Consequently, only the structure of 18.75 mol%Au@TiO_2 displayed sphere Au NPs and present ideal lotus-like morphology, but other samples with lower or higher Au contents presented disordered strctures shown in Fig. 4(b) and (d).

XPS analysis was performed to analyze the surface composition of the 18.75 mol%Au@TiO_2, as shown in Fig. 6. Fig. 6(a) exhibits the wide XPS survey spectra of 18.75 mol%Au@TiO_2 nanocomposites, revealing two peaks at 284 and 531 eV, which can be attributed to C 1 s and O 1s, respectively. Furthermore, 18.75 mol%Au@TiO_2 composites exhibit several bands associated with Ti2p and Au4f,

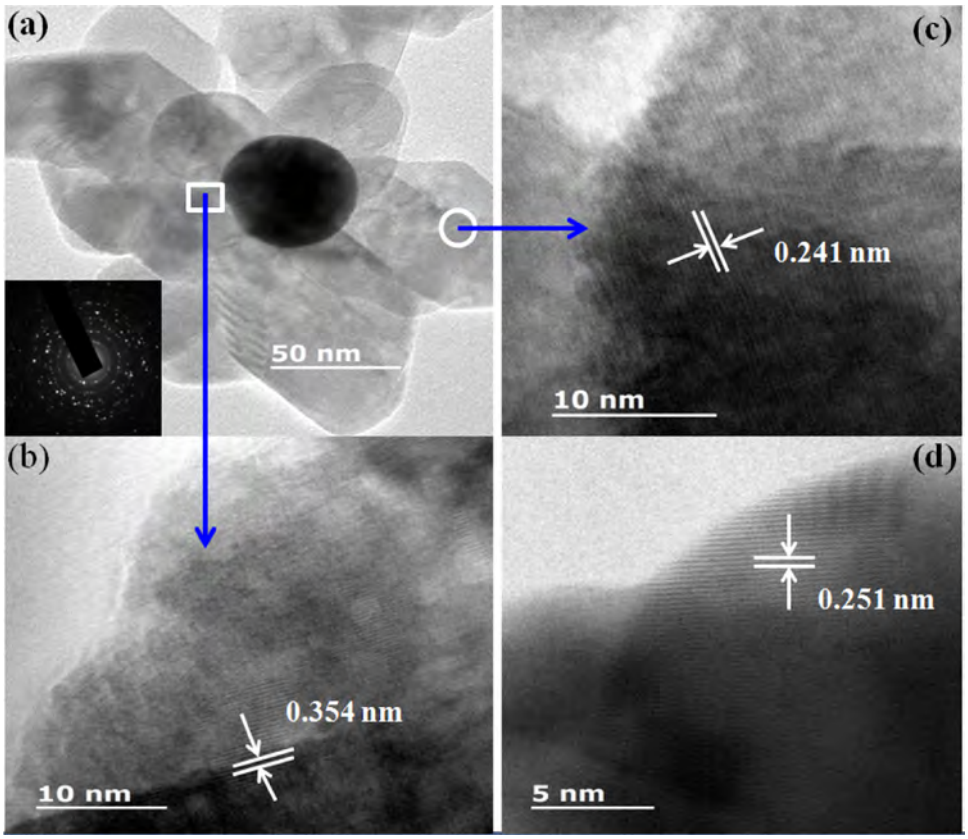

Fig. 5. (a) TEM images of individual 18.75 mol%Au@TiO_2. (b) HRTEM of root region: rectangular region of Fig. 5(a). (c) HRTEM of external edge: circular region of Fig. 5(a). (d) HRTEM images of Au NPs. The insets in parts (a) is electronic diffraction (ED) pattern of the individual lotus-like Au@TiO_2.

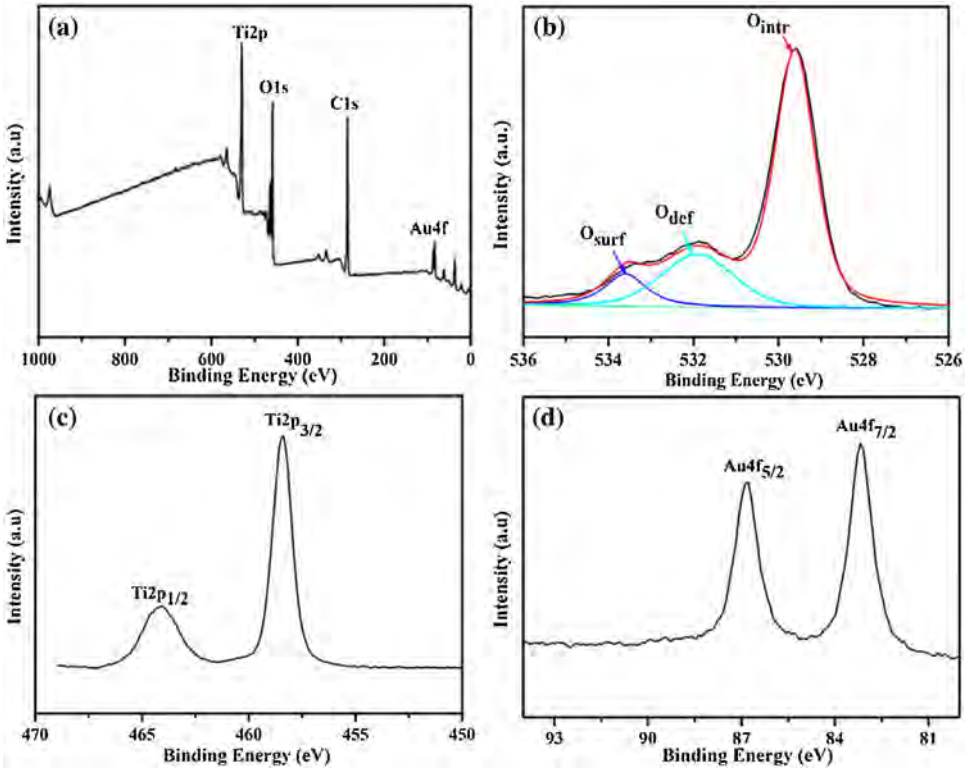

Fig. 6. XPS spectra of 18.75 mol%Au@TiO_2 nanocomposites: (a) wide XPS spectra of Au@TiO_2; (b) O 1s; (c) Ti 2p; (d) Au 4f.

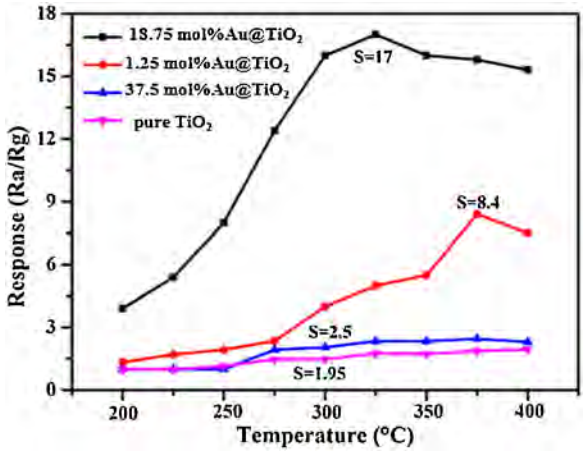

Fig. 7. The responses of the sensors made with pure TiO_2 and Au@TiO_2 to 500 ppm CO at operating temperature in the range of 200 ~ 400 °C.

indicating the presence of Ti and Au element in the hybrid architecture. The O 1 s profiles displayed in Fig. 6(b) can be divided into three peaks of O_{intr}, O_{def} and O_{surf} locating at 529.8, 531.6 and 533.3 eV, respectively. The O_{intr} peak is associated with lattice oxygen in anatase TiO_2, the O_{def} and O_{surf} peaks are assigned to oxygen species in H_2O molecules and Ti—OH or CO_3^{2-} [35]. Fig. 6(c) gives the binding energies at 458.8 and 464.5 eV corresponding to Ti $2p_{3/2}$ and Ti $2p_{1/2}$ [36]. Fig. 6(d) shows binding energies of Au$4f_{7/2}$ at 83.4 and Au$4f_{5/2}$ at 87.0 eV, which are significantly different from $Au^+4f_{7/2}$ (84.6 eV) and $Au^{3+}4f_{7/2}$ (87.0 eV) but similar to $Au^0 4f_{7/2}$ (84.0 eV) [37,38], the negative shift of $Au^0 4f_{7/2}$ (0.6 eV) indicates strong interactions between Au and the TiO_2 framework.

3.2. Gas sensing properties

The effects of operating temperature on sensing properties of TiO_2 and Au@TiO_2 nanocomposites were examined by investigating their responses to CO of 500 ppm. Fig. 7 shows the responses of four sensors at operating temperatures ranging from 200 to 400 °C. It can be easily observed that the responses varied with operating temperature, the differences of optimal operating temperature and sensitivities were significant among these tested sensors. For the sensors made with pure TiO_2 and 37.5 mol%Au@TiO_2, their response to CO shifted slightly with operating temperature, their sensitivities were relatively low with maximal value of 2.5 and 1.95 at 325 and 400 °C, respectively. While for 1.25 and 18.75 mol%Au@TiO_2, their sensitivities increased at the beginning, reached the climax, then decreased gradually with operating temperatures, and their optimal operating temperature reduced greatly compared with pure TiO_2.

In particular, the optimal operating temperature of the sensors made with 18.75 mol%Au@TiO_2 lotus-like materials is lower from 400 °C of pure TiO_2 sensors to 325 °C. More importantly, the response of 18.75 mol%Au@TiO_2 sensors is always far higher than that of other sensors at the same corresponding temperature in the full temperature range, its maximal response at 325 °C rise up to 17 which is 8.5 times higher than that of sensors made with pure TiO_2. These results demonstrate clearly that Au NPs attached onto the center of TiO_2 forming lotus-like structure materials can dramatically improve the sensing performances of pure TiO_2, not only lowering the optimal operating temperature but also enhancing the response. It is worth noting that the amount of Au addition has an optimal value of 0.1875 in this study.

Fig. 8(a) exhibited the typical response transient of the sensor based on 18.75 mol%Au@TiO_2 using actual resistance values upon exposure of various concentration of CO gas. When exposed to CO, the sensor resistance rapidly decreased, implying *n*-type response of our sensor. As increased CO concentration, the change of sensor resistance is promoted clearly. And the lowest detection concentration of CO can reach 10 ppm. Remarkably, the decrease rate of sensor resistance become slowly when CO concentration was more than 200 ppm due to nearing saturation of the system. Moreover, the sensor resistance can return to its original value after a response and recovery cycle, indicating an excellent stability. Especially, the detection limit of the 18.75 mol%Au@TiO_2 sensor can be reduced to 10 ppm with higher response of 1.75. To our knowledge, this is the first demonstration of CO gas sensing by TiO_2-based sensors, where the lowest detection limit has been achieved at relatively simple approach [39]. The response of pure TiO_2 and Au@TiO_2-based gas sensors for variable CO concentration (10 ~ 1000 ppm) at their respective optimal operating temperatures are compared and exhibited in Fig. 8(b). As can be seen from this figure, all the sensors exhibit enhanced responses with the increasing CO concentration, but there are significant differences among the response. It is easily observed that the lotus-like 18.75 mol%Au@TiO_2 sensor had the highest response in the full concentration range of CO among all the sensors, which is similar to the results in the full temperature range shown in Fig. 7. Moreover, the response curve of lotus-like 18.75 mol%Au@TiO_2 sensor shows a broad dynamic linear range from 10 to 1000 ppm, while that of pure TiO_2 and 37.5 mol%Au@TiO_2 sensors show trend of slow increase which indicated that they are insensitive to CO gas.

The dynamic response-recovery curves of the 18.75 mol%Au@TiO_2 sensor to 90 ppm CO at 325 °C are presented in Fig. 9(a). It is obvious that the resistance dropped sharply with the introduction of CO and then held wave nearby a constant value, while the resistance rose rapidly and returned to its initial value with the release of CO. The measured response and recovery time of the above mentioned sensor are 3 and 6 s, respectively. Reproducibility is also checked by repeating the response for 100 ppm CO five times as shown in the inset of Fig. 9(a). It can be noticed that the resistance in air and 90 ppm CO gas kept amost at the original value even after 5 times of repeated operation, which confirmed that the 18.75 mol%Au@TiO_2 sensor with lotus-like structure had good reversibility. The stability test of the sensors were checked and depicted in Fig. 9(b). The actual resistance of the as-fabricated sensors to 90 ppm CO at 325 °C is investigated in a series day. It was found that mild variations were detected in the resistance values of the sensor, which revealed that the sensors exhibited excellent stability.

For comparison, the response and recovery time of all the four sensors of pure TiO_2 and Au@TiO_2 are summarized in Table 2. The values listed in the table indicate that the response and recovery characteristics of Au@TiO_2 based sensors are superior to the pure TiO_2-based sensors.

Selectivity is an important criterion of evaluating gas sensors, especially in the presence of multiple gases possessing similar physicochemical properties. Here, the selectivity of pure TiO_2 and Au@TiO_2-based sensors was also inspected carefully by checking gases of 100 ppm at 325 °C. Fig. 10. reveals the responses of sensors to CO, H_2, NH_3, NO. It is clearly observed that the 18.75 mol%Au@TiO_2 sensor exhibits the largest response to CO

Table 2
Response and recovery time of pure TiO_2 and Au@TiO_2-based sensors to 100 ppm CO at optimal operating temperatures.

Sensors	Response time (Second)	Recovery time (Second)
18.75 mol%Au@TiO_2	5	8
1.25 mol%Au@TiO_2	10	15
37.5 mol%Au@TiO_2	15	20
Pure TiO_2	20	30

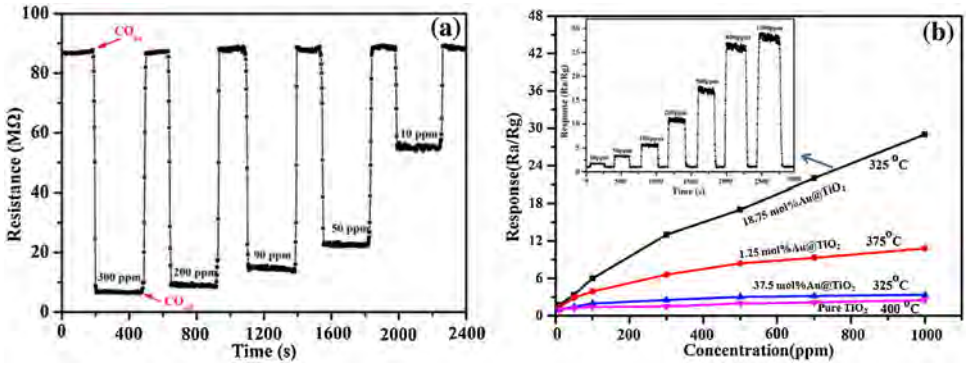

Fig. 8. (a) Dynamic sensing transient response of 18.75 mol%Au@TiO_2 sensors versus 10–300 ppm CO concentration at its optimal operating temperatures (b) The response of the pure TiO_2 and Au@TiO_2 to different CO concentration at their respective optimal operating temperatures. Insert: The response of 18.75 mol%Au@TiO_2 to different CO concentration.

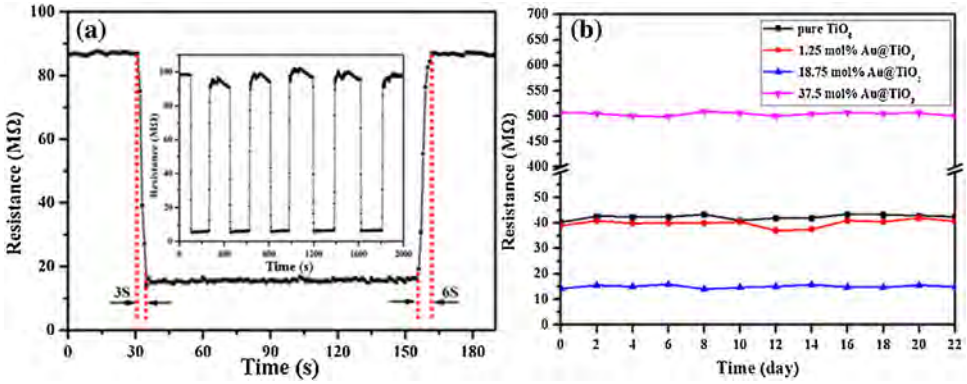

Fig. 9. (a) Dynamic response-recovery curves of 18.75 mol%Au@TiO_2 nanocomposites to 90 ppm CO at 325 °C. (b) The actual resistances of the four sensors upon exposure of 90 ppm CO at 325 °C after storage for different time periods.

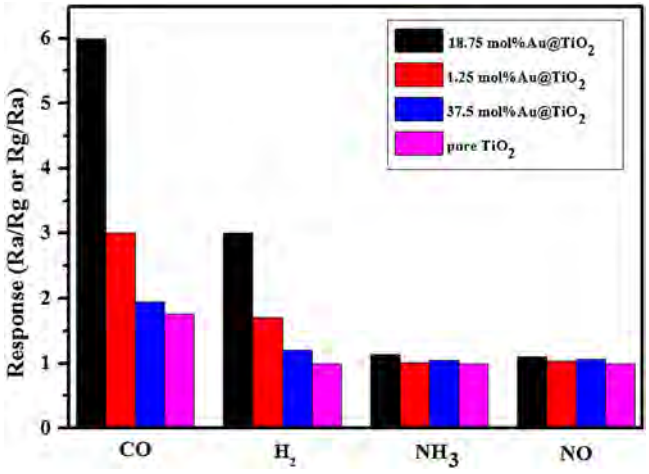

Fig. 10. Response to various gases (100 ppm) of pure TiO_2 and Au@TiO_2-based sensores at 325 °C.

among these gases. The response of pure TiO_2 sensors to various gases is very low and at almost the same level.

A comparable survey of the sensing performances between the sensors in this current work and other TiO_2-based sensors reported in the literature is listed in Table 3. From the table, six kinds of sensors based pure-TiO_2 with different morphology were assessed to detect CO of various concentrations, but their sensing properties including sensitivity, operating temperature and response/recovery characteristics are relatively poor. With the incorporation of Au onto TiO_2, their sensing performances can be improved to some extent. Particularly, considering comprehensively the operating temperature, sensitivity, selectivity, response and recovery time, it is apparent that the sensors fabricated from 18.75 mol%Au@TiO_2 lotus-like materials exhibited the optimally integrative sensing properties toward CO. Therefore, the sensor based on 18.75 mol%Au@TiO_2 lotus-like materials had more advantages than those in the reported literatures.

The foundation that TiO_2 can be used as sensor materials is owing to the presence of inherent oxygen vacancy in its crystal [45], implying Ti has more plus charge while oxygen has minus charge. When TiO_2 is exposed to air, oxygen species could firstly be adsorbed onto the surface of TiO_2, and are ionized into adsorbed O^- and O^{2-} by capturing free electrons from the conductance band of TiO_2, so TiO_2 shows higher resistance in air [20]. While the sensor is exposed to a target gas of CO in this case, CO will react with the adsorbed O^- and O^{2-} leading to the release of electrons, then the resistance of the sensor will be lowered. As mentioned above, the sensor from Au@TiO_2 composite, particularly the louts-like 18.75 mol%Au@TiO_2 exhibited improved response and reduced optimal operating temperature, compared with the sensor from pure TiO_2 leaf. The enhanced response of Au@TiO_2 composites can be contributed mainly to the enhanced adsorption of CO in the presence of Au [46] and the catalytic activity of Au NPs [47,48]. Firstly, the presence of Au facilitates the adsorption of CO. Some positively charged or vacant sites in Au lattice and the other peripheral sites adjacent to TiO_2 support, are regarded as the preferential sites for CO adsorption and the formation of carbonate species [49]. Secondly, many researchers have confirmed that Au NPs can boost the response of metal oxides owing to its electronic and chemical sensitization [50–52]. The electric sensitization means the increase

Table 3
Comparsion investigation on the sensing performance of TiO_2-based gas sensors between this work and reported results in the literature.

Sensingmaterials	Morphology	CO Conc.(ppm)	Operaingtemp. (°C)	Sensitivity(Ra/Rg)	Response/Recovery time(s)	Ref.
TiO_2	thick film	1000	500	3.3	–/–	[12]
TiO_2	nanoplate	10	300	1.5	–/–	[23]
TiO_2	nanotubes	500	500	8	–/–	[24]
TiO_2	nanoporous	100	450	1.2	–/–	[40]
TiO_2	xerogel film	50	300	2.8	18/42	[41]
TiO_2	nanofibers	25	200	4.4	35/86	[42]
Au@TiO_2	nanoparticle	1000	600	1.21	fast/fast	[39]
Au@TiO_2	nanocrystalline	500	500	8	–/–	[43]
Au@TiO_2	lotus-like	500	325	17	8/12	This work
Au@TiO_2	lotus-like	500	200	4	11/50	This work
Au@TiO_2	flims	100	300	2	11.6/39	[44]
Au@TiO_2	lotus-like	90	325	5	3/6	This work

of baseline resistance in Au@TiO_2 composites in comparison with pure TiO_2 [39], because Au NPs can acts as an electron acceptor on TiO_2 surface. Thus, the change in resistance is larger leading to the increase in response. In chemical sensitization, Au NPs provide effective adsorption sites to bind and dissociate oxygen molecules, resulting in a larger degree of electron extractions from the conduction band of TiO_2 than the pristine TiO_2 [47]. Based on these, the response of sensor made with Au@TiO_2 composites is superior to that of sensors made with pure TiO_2, which is consist with the results in our case.

Furthermore, the catalytic activity of Au is strongly dependent on the size and shape of Au NPs supported on TiO_2. The CO oxidation will be enhanced by facilitating the migration of CO molecules, if the Au particles supported on TiO_2 are small in diameter and nearly spherical [53]. It has also been proposed that the oxidation sites are located at the perimeter of the interface between Au and the support [49]. As shown in Fig. 4, the Au NPs in 18.75 mol%Au@TiO_2 displayed sphere while the Au NPs in 1.25 and 37.5 mol%Au@TiO_2 look like ellipse or egg, and the 18.75 mol%Au@TiO_2 composites present smaller Au core size and ideal lotus-like morphology. It is obvious that the 18.75 mol%Au@TiO_2 possess the optimal structure for CO sensing. On the other hand, Au NPs will aggregate when the Au molar ratio was increased to 0.375 depicted in Fig. 4(d), the excessive thickness of Au NPs would obstruct the penetration of the detected gas to the gas sensing matrix [54], which will result in the loss of response. Consequently, the introduction of Au into the TiO_2 matrix can enhance the sensing performance of TiO_2-based sensors, and there is an optimal amount of Au supported on TiO_2 in which the suitable structure of Au@TiO_2 with improved sensing performance can be achieved.

4. Conclusions

In summary, lotus-like Au@TiO_2 heterostructures were successfully fabricated by one step hydrothermal reaction without surfactant by controlling the ratio of Au to TiF_4. The obtained samples were applied as sensor materials for detecting gases including CO and H_2, NO, etc, and their gas sensing properties were examined. It is found that the lotus-like Au@TiO_2 based sensors shown the best outstanding sensing performance to CO compared with other samples. The response of lotus-like Au@TiO_2 rose to 17 for 500 ppm CO at 325 °C, which is 8.5 times of that of pure TiO_2. Moreover, the selectivity, the response and recovery time are improved greatly, which confirmed the lotus-like Au@TiO_2 nanostructures had promising potential in gas sensing applications. The enhancement mechanism of sensing performance of lotus-like Au@TiO_2 are also investigated, which is contributed to the unique lotus-like nanostructure and the catalytic activity of Au NPs.

Acknowdgements

This work was financially supported by the funding support of Science & Technology program of Wuhan Science and Technology Bureau (2015060202010121), the National Natural Science Foundation of China (No. 21471120), International Cooperation Foundation of Hubei Province (2012IHA00201), Educational Commission of Hubei Province of China (T201306).

References

[1] G.F. Fine, L.M. Cavanagh, A. Afonja, R. Binions, Metal oxide semi-conductor gas sensors in environmental monitoring, Sensors 10 (2010) 5469–5502.
[2] K. Wetchakun, T. Samerjai, N. Tamaekong, C. Liewhiran, C. Siriwong, V. Kruefu, A. Wisitsoraat, A. Tuantranont, S. Phanichphant, Semiconducting metal oxides as sensors for environmentally hazardous gases, Sens. Actuators B 160 (2011) 580–591.
[3] L. Xiao, S.M. Shu, S.T. Liu, A facile synthesis of Pd-doped SnO_2 hollow microcubes with enhanced sensing performance, Sens. Actuators B 221 (2015) 120–126.
[4] M. Graf, D. Barrettino, S. Taschini, C. Hagleitner, A. Hierlemann, H. Baltes, Metal oxide-based monolithic complementary metal oxide semiconductor gas sensor microsystem, Anal. Chem. 76 (2004) 4437–4445.
[5] H.-C. Chiu, C.-S. Yeh, Hydrothermal synthesis of SnO_2 nanoparticles and their gas-sensing of alcohol, J. Phys. Chem. C 111 (2007) 7256–7259.
[6] J. Zhang, S.R. Wang, M.J. Xu, Y. Wang, B.L. Zhu, S.M. Zhang, W.P. Huang, S.H. Wu, Hierarchically porous ZnO architectures for gas sensor aplication, Cryst. Growth Des. 9 (2009) 3532–3537.
[7] X. Hu, J.C. Yu, J. Gong, Q. Li, G. Li, α-Fe_2O_3 nanorings prepared by a microwave-assisted hydrothermal process and their sensing properties, Adv. Mater. 19 (2007) 2324–2329.
[8] T. Waitz, T. Wagner, T. Sauerwald, C.-D. Kohl, M. Tiemann, Ordered mesoporous In_2O_3: synthesis by structure replication and application as a methane gas sensor, Adv. Funct. Mater. 19 (2009) 653–661.
[9] X.-L. Li, T.-J. Lou, X.-M. Sun, Y.-D. Li, Highly sensitive WO_3 hollow-sphere gas sensors, Inorg. Chem. 43 (2004) 5442–5449.
[10] X.J. Wan, J.L. Wang, L.F. Zhu, J.N. Tang, Gas sensing properties of Cu_2O and its particle size and morphology-dependent gas-detection sensitivity, J. Mater. Chem. A 2 (2014) 13641.
[11] P. Rai, S.M. Majhi, Y.-T. Yu, J.-H. Lee, Noble metal@metal oxide semiconductor core@shell nano-architectures as a new platform for gas sensor applications, RSC Adv. 5 (2015) 76229–76248.
[12] A.M. Ruiz, G. Sakai, A. Cornet, K. Shimanoe, J.R. Morante, N. Yamazoe, Microstructure control of thermally stable TiO_2 obtained by hydrothermal process for gas sensors, Sens. Actuators B 103 (2004) 312–317.
[13] J. Schneider, M. Matsuoka, M. Takeuchi, J.L. Zhang, Y. Horiuchi, M. Anpo, W.D. Bahnemann, Understanding TiO_2 photocatalysis: mechanisms and materials, Chem. Rev. 114 (2014) 9919–9986.
[14] T. López-Luke, A. Wolcott, L.-p. Xu, S.W. Chen, Z.H. Wen, J.G. Li, E.De La Rosa, Z.J. Zhang, Nitrogen-doped and CdSe quantum-dot-sensitized nanocrystalline TiO_2 films for solar energy conversion applications, J. Phys. Chem. C 112 (2008) 1282–1292.
[15] S. Banerjee, D.D. Dionysiou, S.C. Pillai, Self-cleaning applications of TiO_2 by photo-induced hydrophilicity and photocatalysis, Appl. Catal. B 176–177 (2015) 396–428.
[16] Y. Ohko, T. Tatsuma, T. Fujii, K. Naoi, C. Niwa, Y. Kubota, A. Fujishima, Multicolour photochromism of TiO_2 films loaded with silver nanoparticles, Nat. Mater. 2 (2003) 29–31.
[17] J. Bai, B.X. Zhou, Titanium dioxide nanomaterials for sensor applications, Chem. Rev. 114 (2014) 10131–10176.
[18] T.-J. Ha, M.-H. Hong, C.-S. Park, H.-H. Park, Gas sensing properties of ordered mesoporous TiO_2 film enhanced by thermal shock induced cracking, Sens. Actuators B 181 (2013) 874–879.

[19] K.M. Garadkar, B.S. Shirke, P.P. Hankare, D.R. Patil, Low cost nanostructured anatase TiO_2 as a H_2S gas sensor synthesized by microwave assisted technique, Sens. Lett. 9 (2011) 526–532.
[20] C. Wang, L. Yin, L. Zhang, Y. Qi, N. Lun, N. Liu, Large scale synthesis and gas-sensing properties of anatase TiO_2 three-dimensional hierarchical nanostructures, Langmuir 26 (2010) 12841–12848.
[21] A. Haidry, P. Schlosser, P. Durina, M. Mikula, M. Tomasek, T. Plecenik, T. Roch, A. Pidik, M. Stefecka, J. Noskovic, M. Zahoran, P. Kus, A. Plecenik, Hydrogen gas sensors based on nanocrystalline TiO_2 thin films, Open Phys. (2011) p1351.
[22] A. Wisitsoraat, A. Tuantranont, E. Comini, G. Sberveglieri, W. Wlodarski, Characterization of n-type and p-type semiconductor gas sensors based on NiO_x doped TiO_2 thin films, Thin Solid Films 517 (2009) 2775–2780.
[23] W. Guo, Q.Q. Feng, Y.F. Tao, L.J. Zheng, Z.Y. Han, J.M. Ma, Systematic investigation on the gas-sensing performance of TiO_2 nanoplate sensors for enhanced detection on toxic gases, Mater. Res. Bull. 73 (2016) 302–307.
[24] M.-H. Seo, M. Yuasa, T. Kida, J.-S. Huh, K. Shimanoe, N. Yamazoe, Gas sensing characteristics and porosity control of nanostructured films composed of TiO_2 nanotubes, Sens. Actuators B 137 (2009) 513–520.
[25] H.G. Moon, Y.-S. Shim, D. Su, H.-H. Park, S.-J. Yoon, H.W. Jang, Embossed TiO_2 thin films with tailored links between hollow hemispheres: synthesis and gas-sensing properties, J. Phys. Chem. C 115 (2011) 9993–9999.
[26] P.G. Hu, G.J. Du, W.J. Zhou, J.J. Cui, J.J. Lin, H. Liu, D. Liu, J.G. Wang, S.W. Chen, Enhancement of ethanol vapor sensing of TiO_2 nanobelts by surface engineering, ACS Appl. Mater. Interfaces 2 (2010) 3263–3269.
[27] R.J. Lu, W. Zhou, K.Y. Shi, Y. Yang, L. Wang, K. Pan, C.G. Tian, Z.Y. Ren, H.G. Fu, Alumina decorated TiO_2 nanotubes with ordered mesoporous walls as high sensitivity NO_x gas sensors at room temperature, Nanoscale 5 (2013) 8569–8576.
[28] J. Li, H.C. Zeng, Size tuning, functionalization, and reactivation of Au in TiO_2 nanoreactors, Angew. Chem. Int. Ed. 117 (2005) 4416–4419.
[29] X.F. Wu, H.Y. Song, J.M. Yoon, Y.T. Yu, Y.F. Chen, Synthesis of core-shell $Au@TiO_2$ nanoparticles with truncated wedge-shaped morphology and their photocatalytic properties, Langmuir 25 (2009) 6438–6447.
[30] T. Hirakawa, P.V. Kamat, Charge separation and catalytic activity of $Ag@TiO_2$ core-shell composite clusters under UV-irradiation, J. Am. Chem. Soc. 127 (2005) 3928–3934.
[31] R. Buonsanti, V. Grillo, E. Carlino, C. Giannini, M.L. Curri, C. Innocenti, C. Sangregorio, K. Achterhold, G.F. Parak, A. Agostiano, D.P. Cozzoli, Seeded growth of asymmetric binary nanocrystals made of a semiconductor TiO_2 rodlike section and a magnetic gamma-Fe_2O_3 spherical domain, J. Am. Chem. Soc. 128 (2006) 16953–16970.
[32] P.D. Cozzoli, T. Pellegrino, L. Manna, Synthesis, properties and perspectives of hybrid nanocrystal structures, Chem. Soc. Rev. 35 (2006) 1195–1208.
[33] F.-h. Lin, R.-a. Doong, Bifunctional Au-Fe_3O_4 heterostructures for magnetically recyclable catalysis of nitrophenol reduction, J. Phys. Chem. C 115 (2011) 6591–6598.
[34] J. Geng, G.-H. Song, X.-D. Jia, F.-F. Cheng, J.-J. Zhu, Fast one-step synthesis of biocompatible ZnO/Au nanocomposites with hollow doughnut-like and other controlled morphologies, J. Phys. Chem. C 116 (2012) 4517–4525.
[35] H. Li, Z. Bian, J. Zhu, Y. Huo, H. Li, Y. Lu, Mesoporous Au/TiO_2 nanocomposites with enhanced photocatalytic activity, J. Am. Chem. Soc. 129 (2007) 4538–4539.
[36] S. Lee, I.-S. Cho, J.H. Lee, D.H. Kim, D.W. Kim, J.Y. Kim, Two-step sol- gel method-based TiO_2 nanoparticles with uniform morphology and size for efficient photo-energy conversion devices, Chem. Mater. 22 (2010) 1958–1965.
[37] J. Li, H.C. Zeng, Preparation of monodisperse Au/TiO_2 nanocatalysts via self-assembly, Chem. Mater. 18 (2006) 4270–4277.
[38] N. Kruse, S. Chenakin, XPS characterization of Au/TiO_2 catalysts: binding energy assessment and irradiation effects, Appl. Catal. A 391 (2011) 367–376.
[39] Y.-S. Kim, P. Rai, Y.-T. Yu, Microwave assisted hydrothermal synthesis of $Au@TiO_2$ core–shell nanoparticles for high temperature CO sensing applications, Sens. Actuators B 186 (2013) 633–639.
[40] E. Tolmachoff, S. Memarzadeh, H. Wang, Nanoporous titania gas sensing films prepared in a premixed stagnation flame, J. Phys. Chem. C. 115 (2011) 21620–21628.
[41] J.-S. Lee, T.-J. Ha, M.-H. Hong, C.-S. Park, H.-H. Park, The effect of multiwalled carbon nanotube doping on the CO gas sensitivity of TiO_2 xerogel composite film, Appl. Surf. Sci. 269 (2013) 125–128.
[42] J.-A. Park, J. Moon, S.-J. Lee, S.H. Kim, T. Zyung, H.Y. Chu, Structure and CO gas sensing properties of electrospun TiO_2 nanofibers, Mater. Lett. 64 (2010) 255–257.
[43] A.M. Ruiz, A. Cornet, K. Shimanoe, J.R. Morante, N. Yamazoe, Effects of various metal additives on the gas sensing performances of TiO_2 nanocrystals obtained from hydrothermal treatments, Sens. Actuators B 108 (2005) 34–40.
[44] D. Buso, M. Post, C. Cantalini, P. Mulvaney, A. Martucci, Gold nanoparticle-doped TiO_2 semiconductor thin films: gas sensing properties, Adv. Funct. Mater. 18 (2008) 3843–3849.
[45] J. Bai, B.X. Zhou, Titanium dioxide nanomaterials for sensor applications, Chem. Rev. 114 (2014) 10131–10176.
[46] D. Buso, M. Post, C. Cantalini, P. Mulvaney, A. Martucci, Gold nanoparticle-doped TiO_2 semiconductor thin films: gas sensing properties, Adv. Funct. Mater. 18 (2008) 3843–3849.
[47] T.A. Baker, X.Y. Liu, C.M. Friend, The mystery of gold's chemical activity: local bonding, morphology and reactivity of atomic oxygen, Phys. Chem. Chem. Phys. 13 (2011) 34–46.
[48] S. Matsushima, Y. Teraoka, N. Miura, N. Yamazoe, Electronic interaction between metal additives and tin dioxide in tin dioxide-based gas sensors, Jpn. J. Appl. Phys. 27 (1988) 1798–1802.
[49] M. Haruta, S. Tsubota, T. Kobayashi, H. Kageyama, M.J. Genet, B. Delmon, Low-temperature oxidation of CO over gold supported on TiO_2, alpha-Fe_2O_3 and Co_3O_4, J. Catal 144 (1) (1993) 175–192.
[50] P. Rai, Y.-S. Kim, H.-M. Song, M.-K. Song, Y.-T. Yu, The role of gold catalyst on the sensing behavior of ZnO nanorods for CO and NO_2 gases, Sens. Actuators B 165 (2012) 133–142.
[51] Y.-T. Yu, P. Dutta, Examination of Au/SnO_2 core-shell architecture nanoparticle for low temperature gas sensing applications, Sens. Actuators B 157 (2011) 444–449.
[52] M.-H. Seo, M. Yuasa, T. Kida, J.-S. Huh, N. Yamazoe, K. Shimanoe, Enhanced gas sensing characteristics of Au-loaded TiO_2 nanotube sensors, Sensor Lett. 9 (2011) 26–30.
[53] G.H. Takaoka, T. Hamano, K. Fukushima, J. Matsuo, I. Yamada, Preparation and catalytic activity of nano-scale Au islands supported on TiO_2, Nucl. Instrum, Methods Phys. Res. Sect. B 121 (1997) 503–506.
[54] H.-W. Kwon, Y.-M. Lim, S.K. Tripathy, B.-G. Kim, M.-S. Lee, Y.-T. Yu, Synthesis of Au/TiO_2 core-shell nanoparticles from titanium isopropoxide and thermal resistance effect of TiO_2 shell, Jpn. J. Appl. Phys. 46 (2007) 2567–2570.

Biographies

Haiyang Liu received her B.S. degree in Hu Bei University of Arts and Science in 2013. She is currently working towards her M.S. degree at Wuhan Institute of Technology supervised by Prof. Shantang Liu. Her research interests focuses on the synthesis of noble metal@semiconducting metal oxides and their applications in gas sensors.

Wei Yang received his PhD degree in analytical chemistry from Wuhan University at 2014. Currently, he is working as a lecturer in the School of Chemistry and Environmental Engineering, Wuhan Institute of Technology. His research focuses on the development of semiconductor gas sensors.

Mingxi Wang received his Ph.D. degree from Tsinghua University in 2013 (Supervisor: Prof. Zhenghong Huang). His Ph.D. research focused on the development of carbon nanomaterials for gas pollutants (NO_x) treatments. He is currently working as an ***Distinguished professor*** of Wuhan Institute of Technology. His research is focused on the design of new semiconductor sensors and nanocarbon materials for gas pollutants detection and remediation.

Li Xiao received her M.S. degree in Chemistry from China University of Geosciences in 2013. She is currently working as a research associate in Prof. Shantang Liu's group at Wuhan Institute of Technology. Now her work mainly focuses on gas sensors based on semiconductor oxides.

Shantang Liu received his Ph.D. degree from Perking University, China in 2000. He did his postdoctoral work at Weizmann Institute of Science, Israel from September 2000 to January 2004. After this, he worked as a postdoctoral researcher at Laval University, Canada from January 2004 to January 2006, and then as a postdoctoral researcher at Virginia Commonwealth University, USA from January 2006 to March 2007. He is currently "Chutian Scholar Program" ***Distinguished professors*** of Wuhan Institute of Technology and focuses his research primarily on sensitive materials, semiconductor sensors and nanocatalysts.